Astron. Astrophys. 70, 487–500 (1978)

ASTRONOMY AND ASTROPHYSICS

Acoustic Waves in the Solar Atmosphere

V. On the Chromospheric Temperature Rise

P. Ulmschneider[1], F. Schmitz[1], W. Kalkofen[2], and H.U. Bohn[1]

[1] Institut für Astronomie und Astrophysik, Am Hubland, D-8700 Würzburg, Federal Republic of Germany
[2] Harvard-Smithsonian Center for Astrophysics, 60 Garden Street, Cambridge, Mass. 02138, USA

Received March 28, 1978

Summary. In this fifth of a series of papers studying large amplitude acoustic waves we use methods developed in previous papers to compute the propagation of acoustic waves into the chromosphere. The temperature minimum is found close to the point of shock formation and the chromospheric temperature rise is determined after the mean quantities reach a steady state. The position of the chromospheric rise depends primarily on the initial acoustic flux. Photospheric temperature enhancement and the temperature depression of 200 to 500 K at the temperature minimum region caused by the nonlinearity of both Planck function and opacity are discussed. The large amplitude of our waves causes mass loss. Amplification of the acoustic flux due to the $\varkappa$-mechanism is found in the region near unity optical depth.

Key words: solar chromosphere — acoustic heating — mass loss — $\varkappa$-mechanism

1. Introduction

In previous papers of this series on acoustic waves in the solar atmosphere we have described our hydrodynamic code (Ulmschneider et al., 1977a, Paper I) and the treatment of radiative damping (Kalkofen and Ulmschneider, 1977, Paper II). In Paper III (Ulmschneider and Kalkofen, 1977) these methods were used to compute the development of acoustic waves in the solar photosphere. From these calculations we have obtained shock formation heights and acoustic fluxes at the top of the photosphere. Our present work continues these computations into the chromosphere with the aim to eventually produce the observed temperature rise. Note that in our work we will use the term chromosphere to describe the layer between the temperature minimum and the level where hydrogen ionizes. To our knowledge the present work is the first attempt to construct model chromospheres with time dependent means. Time independent chromospheric models have been computed by Jordan (1969), Ulmschneider (1971a), Kaplan et al. (1973), and by Marik (1975). A comparison of the results of these authors with our present work is given in Sect. 3i.

In Paper III to accurately find the shock formation height we have used a perturbation method for the treatment of radiation damping. The advantage of this method is that highly accurate non grey radiative equilibrium or semi-empirical models of the solar photosphere may be used as ambient atmosphere in which the acoustic waves propagate. A radiation hydrodynamic code using grey opacity however will modify such an ambient atmosphere and in absence of wave motion will always aim to generate a grey radiative equilibrium model (c.f. Paper II). For this reason the perturbation method subtracts radiation terms of zeroth order in the energy equation to ensure the time independence of the ambient atmosphere. In cases as in Paper III, where the disturbances due to the wave are small, the linearization inherent in the perturbation treatment is entirely justifiable. It is highly doubtful however whether in the chromosphere where the wave amplitudes are no longer small and for instance the opacity variation across the shock front becomes comparable to the ambient opacity, a perturbation treatment is still permissible. For this reason in the present work we do not use the perturbation treatment but rather employ the full zeroth order radiation method described in Paper II. The disadvantage of this procedure is that we go far below the state of the art in construction of model photospheres and our result will therefore not be very realistic. The photospheric temperature distribution for instance shows less agreement with observation (c.f. Fig. 6). The advantage of this method however is that it allows a selfconsistent treatment independent of any initial or ambient atmosphere. It permits further a much clearer insight into the basic physics of stellar chromospheres, especially the chromospheric energy balance between radiation and shock heating.

Send offprint requests to: P. Ulmschneider

Table 1. Initial grey radiative equilibrium model based on the Kurucz (1978) opacity. x is geometrical height, T temperature, P_{RE} gas pressure, S_0 specific entropy and τ optical depth. For the initial grey equilibrium model based on the opacity of Eq. (26) add the values in brackets, everywhere add $\Delta x = 5.5$ km to the x scale and use τ_A for the optical depth

x (km)	T_{RE}(K)	p_{RE}(dyn/cm^2)	S_0(erg/g K)	τ	τ_A
− 37	7424 (−4)	1.72 E5	−6.36 E8	3.00 E0	3.00 E0
23	5680 (+63)	1.14 E5	−6.53 E8 (−0.02 E8)	6.49 E-1	7.04 E-1
142	4888 (−16)	4.25 E4	−6.14 E8 (+0.01 E8)	9.53 E-2	8.09 E-2
268	4729 (−2)	1.39 E4	−5.47 E8	1.20 E-2	1.07 E-2
392	4708	4.48 E3	−4.76 E8	1.50 E-3	1.49 E-3
517	4705	1.45 E3	−4.04 E8	1.93 E-4	2.09 E-4
641	4705	4.67 E2	−3.31 E8	2.78 E-5	2.92 E-5
765	4705	1.51 E2	−2.59 E8	4.79 E-6	4.09 E-6
890	4705	4.87 E1	−1.87 E8	1.01 E-6	5.70 E-7
1014	4705	1.57 E1	−1.14 E8	2.45 E-7	7.69 E-8
1138	4705	5.08 E0	−4.22 E7	4.61 E-8	7.69 E-9

In Sect. 2 we describe our methods of computation. Sect. 3 displays the results and gives a discussion. Sect. 4 summarizes our conclusions.

2. Method of Computation

a) Initial Atmosphere

The method of computation of acoustic waves in the solar atmosphere has been outlined in Papers I, II, III, and will not be repeated here. We use a Lagrangian frame with coordinates specifying the initial geometric height of mass elements in the atmosphere. The method of characteristics which we use employes Atlas interpolation as described by Ulmschneider et al. (1977b) and by Hammer and Ulmschneider (1978, Paper IV). For the initial atmospheric model we take a grey radiative equilibrium temperature distribution

$$T^4 = \tfrac{3}{4}\, T_{\rm eff}^4 (\tau + \mu), \tag{1}$$

which together with the equation of hydrostatic equilibrium

$$dp = -\rho g dx, \tag{2}$$

and with

$$d\tau = -\rho \varkappa dx, \tag{3}$$

determines the initial state. Here g is the surface gravity, $T_{\rm eff} = 5800$ K the effective temperature, $\mu = 1/\sqrt{3}$ the angle cosine, p the gas pressure, ρ the density, τ the optical depth and x the geometrical height. $\varkappa$ is the grey absorption coefficient per gram for which either the Rosseland table of Kurucz (1978) or an H^- approximation formula given by Eq. (26) was used. The initial models obtained this way are shown in Table 1. Any grey radiative temperature distribution because it neglects the effect of convection becomes unrealistically steep at large τ. To avoid problems with a very steep temperature gradient and with a density inversion we have assumed that our lower boundary is at $\tau_1 = 3$. The wave enters this lower boundary by specifying the piston velocity u_1 and the outgoing intensity I_1^+.

We have

$$u_1 = -u_0 \sin\left(\frac{2\pi}{P} t\right), \tag{4}$$

where t is the time, P the wave period and

$$u_0 = \left(\frac{2 F_{M0}}{\rho_1 c_1}\right)^{1/2}. \tag{5}$$

Here F_{M0} is the initial acoustic flux, ρ_1 the density and c_1 the sound velocity at the lower boundary. (Note that we have discontinued to use the awkward notation πF_M for the acoustic flux and adopt F_M instead). For the outgoing intensity we assume

$$I_1^+ = B_1 + \frac{3\sigma T_{\rm eff}}{4\pi}\mu, \tag{6}$$

where

$$B_1 = \frac{\sigma}{\pi} T_1^4, \tag{7}$$

is the Planck function and T_1 the temperature at the lower boundary. σ is the Stefan-Boltzmann constant. Note that we have neglected small perturbations of I_1^+ caused by the wave. This is permissible in the solar case because of the small amplitude of our waves.

b) Treatment of Radiation Damping

The treatment of radiation damping has been discussed in Paper II and will thus not be repeated here. There are some modifications however for the treatment of grid points which are close to shock points and for grid points when the shock is close to the upper boundary. These modifications are discussed in the appendix. Assuming LTE and with known boundary conditions for the specific intensity we integrate the transfer equation and for every grid or shock point obtain the radiative

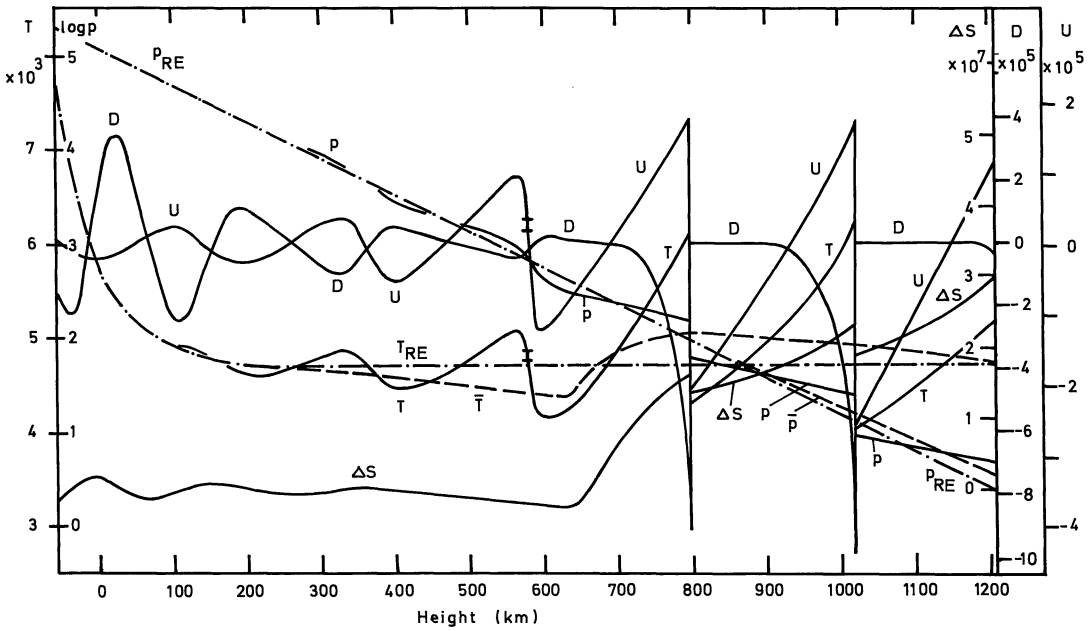

Fig. 1. Acoustic wave of period $P=30$ s with an initial flux $F_{Mo}=5.0$ E7 erg/cm^2 s at time $t=645$ s computed with Kurucz' (1978) opacity as function of Euler height x (km). T(K)=temperature, T_{RE} initial radiative equilibrium temperature, $\bar{T}$ time averaged temperature, p(dyn/cm^2) gas pressure, p_{RE} initial radiative equilibrium pressure, $\bar{p}$ time averaged pressure, ΔS (erg/g K) entropy difference relative to the initial atmosphere, D(erg/g K s) radiative damping function, U(cm/s) gas velocity. At $x=590$ km a shock (indicated) has just been inserted. The shock Mach numbers from the left to right are $M_s=1.014$, 1.44, 1.54

flux derivative

$$\frac{dF_R}{dx}=-4\pi\varkappa\rho(J-B), \tag{8}$$

and the radiative damping function

$$D\equiv\frac{dS}{dt}\bigg|_R=-\frac{1}{\rho T}\frac{dF_R}{dx}=\frac{4\pi\varkappa}{T}(J-B), \tag{9}$$

describing the change in time of the specific entropy S. J is the mean intensity, B the Planck function and T the temperature. Note that in order to avoid an awkward notation for the mechanical flux we denote the radiative flux by F_R. In previous work this quantity is often denoted by πF or by $4\pi H$.

c) Shock Finding Procedure

For the shock finding procedure we use the method outlined in Paper III. This method, called old method in the work of Ulmschneider et al. (1977b), is sufficiently accurate for the Sun. Moreover if care is taken that the old method does not predict the shock too late no harm is done if the shock is introduced too early. In these cases we found that the shock does not develop much strength and therefore does not dissipate.

d) Transmitting Boundary Condition for Shocks

As described in Paper I we use a transmitting boundary condition for the upper boundary. The transmission of the shock requires special care. If the shock comes close to the upper boundary the C^- characteristic emanating from the head of the shock intersects the upper boundary. As the shock overtakes disturbances travelling along C^+ in the front shock region the boundary point, using a C^+ characteristic, can be computed without difficulty regardless of how close the shock has approached the boundary. The physical condition at the intersection point of the C^- characteristic of the shock head with the boundary can thus be interpolated knowing the solution at the boundary at both the new and the old times. If the shock comes so close that within the next time step it would cross the boundary we iterate on the time step such that the shock at the next time coincides exactly with the upper boundary. With this the physical state in front of the shock is already specified. The quantities behind the shock may now be computed using the remaining C^+ characteristic and the Hugoniot relations. At the subsequent time the shock is considered to be already transmitted.

3. Results and Discussion

a) Points of Shock Formation and the Temperature Minima

In our computations for reasons discussed in Sect. 3*g* we have used two different opacities, the Kurucz (1978) opacity table or an opacity given by Eq. (26). With given initial acoustic flux F_{M0} and wave period P the development of acoustic waves have been calculated

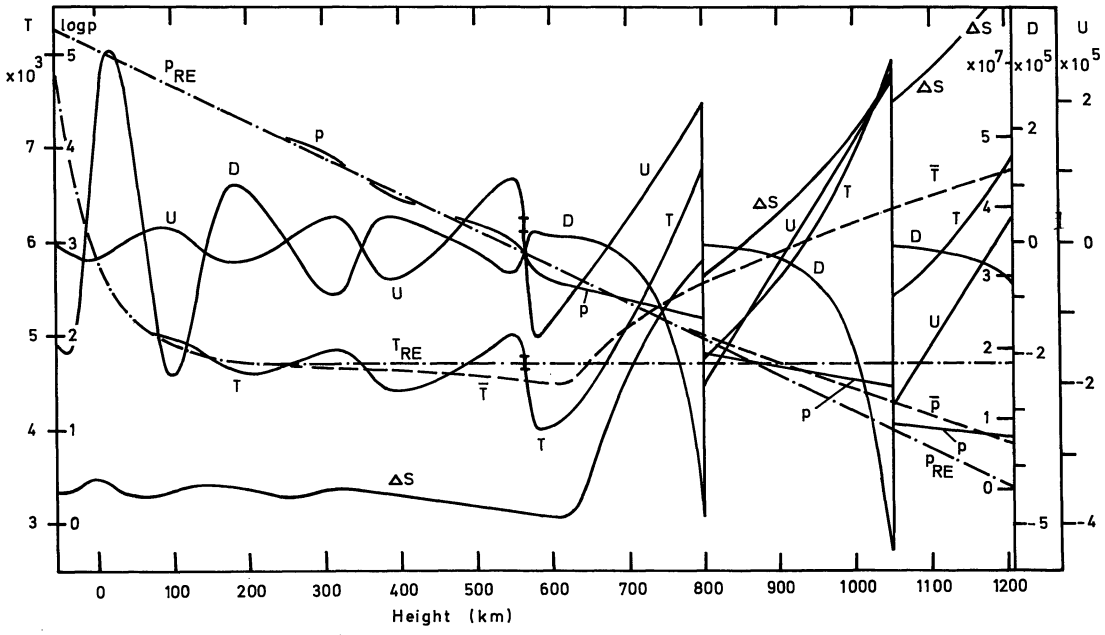

Fig. 2. Same as Fig. 1 however with an opacity after Eq. (26) at time $t=1033$ s. At $x=570$ km a shock (indicated) has just been inserted. The shock Mach numbers from left to right are $M_S=1.015, 1.43, 1.47$

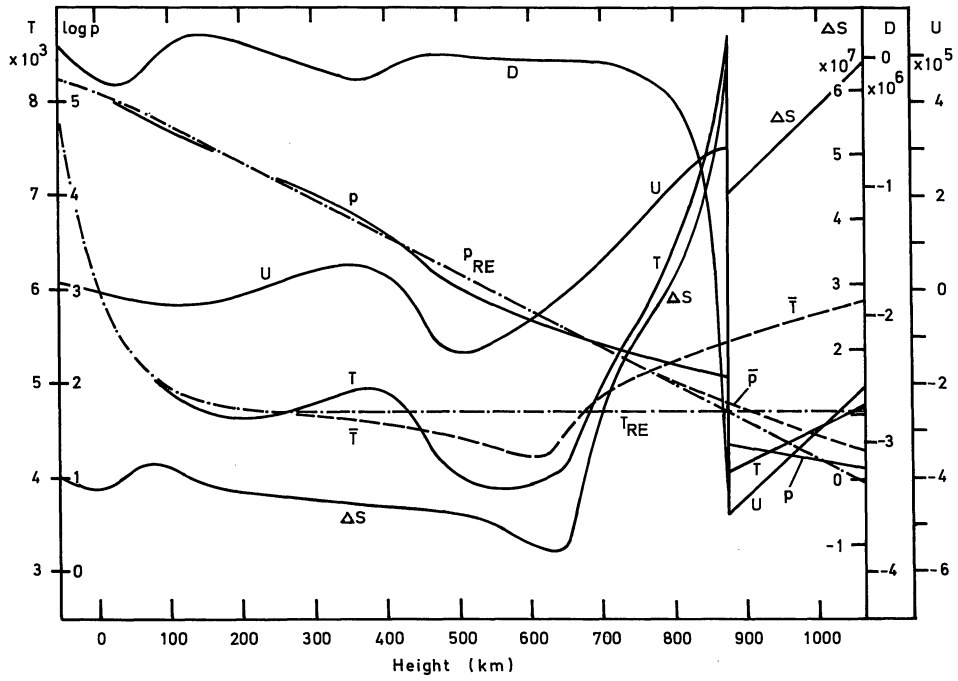

Fig. 3. Same as Fig. 1 however with period $P=60$ s and with an opacity after Eq. (26) at time $t=817$ s. The Mach number of the shock is $M_S=2.04$

with the methods of Sect. 2 starting with the grey radiative equilibrium atmosphere shown in Table 1. Figs. 1–3 and Table 3 display the results. The heights of shock formation X_{SH} and the acoustic fluxes F_{MS} at this point are compared in Table 3 with the values $X_{SH}^{(1)}$, $F_{MS}^{(1)}$ of Ulmschneider and Kalkofen (1977). There are only minor differences between these and our values. The greater shock height in our present work is explained by the hotter temperature distribution (see Fig. 6). Greater shock heights in turn lead to smaller acoustic fluxes F_{MS}. For a detailed discussion of the dependence of the quantities X_{SH} and F_{MS} on initial flux and period see Paper III. Figs. 1, 2, 3, and 6 show the height X_{TM} and acoustic flux F_{MT} at the minimum of the time averaged temperature $\bar{T}$. It is seen that the heights X_{TM} and X_{SH} are quite close, $X_{TM}-X_{SH}\simeq 50$ km or about 4 grid

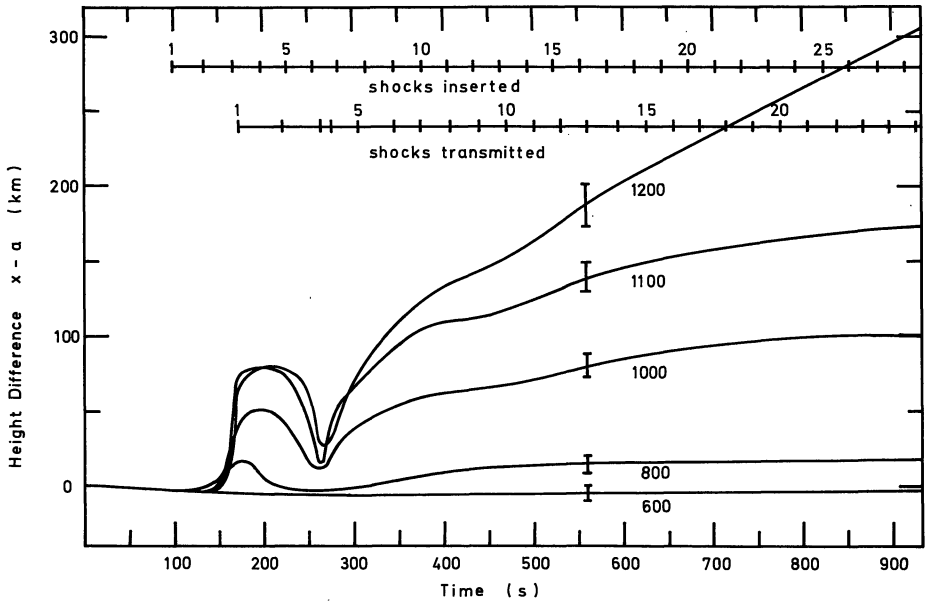

Fig. 4. Height difference x-a (km) between actual and initial position of gas particles as function of time. The gas particles are identified by the Lagrange height a (km). The scatter of x-a around the mean curve is indicated by error bars. Times at which shocks are inserted or transmitted are indicated. The values are for the computation shown in Fig. 2

points. This confirms the rough identification of the temperature minimum with the shock height for the Sun as assumed in Paper III. This close correlation is however not valid for stars like Arcturus (c.f. Ulmschneider et al., 1978) where because of radiative damping there is a considerable distance between X_{TM} and X_{SH}. Due to the small distance between shock height and temperature minimum for the Sun the acoustic flux F_{MT} is only slightly less than F_{MS}. This is again quite different from the case of Arcturus (c.f. Ulmschneider et al., 1978) where the flux difference $F_{MS}-F_{MT}$ is large.

b) Photospheric Temperature Enhancement

In Figs. 1, 2, 3, and 6 at low height the time averaged temperature $\bar{T}$ is essentially identical to the radiative equilibrium temperature T_{RE}. This may be explained by considering the photospheric energy balance. It is easy to show that in the photosphere and low chromosphere energy loss due to viscosity, thermal conduction or solar wind is unimportant (Ulmschneider, 1970). The latter is valid after steady state, c.f. Sect. 3e, has been reached. As derived in Appendix B we have

$$\overline{\frac{dF_M}{dX}}+\overline{\frac{dF_R}{dx}}=0, \tag{10}$$

where bars denote time averages over a wave period. With Eq. (8) we find

$$\overline{\frac{dF_M}{dx}}=4\pi\,\overline{\varkappa\rho(J-B)}. \tag{11}$$

In the photosphere at $x<300$ km after Fig. 5 the left hand side of Eq. (11) for the 30 s wave is about -1.5 erg/cm^3 s whereas the term $4\pi\varkappa\rho J$ at the right hand side after Tables 1, 2, and 4 varies between 10^5 and 10^2 erg/cm^3 s. We thus may neglect the l. h. side of Eq. (11) and as the variation of $\varkappa\rho$ is small have

$$\bar{B}\simeq\bar{J}. \tag{12}$$

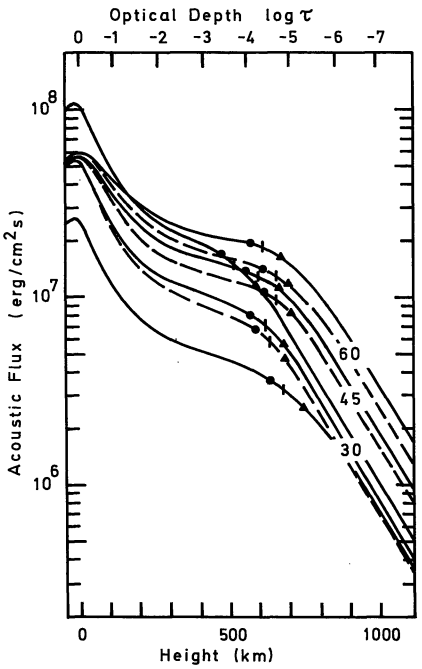

Fig. 5. Acoustic flux F_M as function of Euler height x for waves of various initial fluxes and wave periods indicated in s. Calculations with Kurucz (1978) opacity are shown dashed and with the opacity of Eq. (26) are shown drawn. Heights of shock formation x_{SH}(●), of temperature minima x_{TM}(|) and of full development of the shock x_{FD}(▲) are indicated

Table 2. Mean intensity J (erg/cm^2 s sterad) at various Lagrange heights a (km) and times t(s). J_{RE} is the mean intensity of the initial radiative equilibrium atmosphere of Table 1

	a (km)				
t(s)	50.4	261	478	789	1100
960.6	1.3367 E10	9.0161 E9	8.8935 E9	8.8892 E9	8.8890 E9
967.4	1.3368 E10	8.9181 E9	8.7805 E9	8.7745 E9	8.7743 E9
975.3	1.3375 E10	8.9617 E9	8.8207 E9	8.8149 E9	8.8147 E9
983.2	1.3387 E10	9.0736 E9	8.9457 E9	8.9411 E9	8.9410 E9
989.9	1.3364 E10	9.0274 E9	8.9054 E9	8.9013 E9	8.9011 E9
J_{RE}	1.3374 E10	8.9856 E9	8.8517 E9	8.8465 E9	8.8464 E9

Table 3. As function of initial acoustic flux F_{Mo} and wave period P, the heights of shock formation x_{SH}, of temperature minima x_{TM} and full development of the shock x_{FD} are shown together with the acoustic fluxes at shock formation F_{MS} and at the temperature minimum F_{MT}. The gradient of the time averaged temperature dT/dx is shown at $x=900$ km and the shock Mach number M_S at 1000 km. (1) indicates values taken from Paper III. The values shown are for calculations using the opacity of Eq. (26), while values in brack ets are for Kurucz' (1978) opacity

P(s)	30	30	30	45	60
F_{Mo}(erg/cm^2 s)	2.5 E7	5.0 E7	1.0 E8	5.0 E7	5.0 E7
x_{SH}(km)	650	570 (590)	480	560 (620)	580 (620)
$x_{SH}^{(1)}$ (km)	600	530	460	530	—
F_{MS}(erg/cm^2 s)	3.7 E6	7.9 E6 (6.6 E6)	1.7 E7	1.4 E7 (1.1 E7)	1.8 E7 (1.4 E7)
$F_{MS}^{(1)}$ (erg/cm^2 s)	5.2 E6	1.0 E7	2.0 E7	1.7 E7	—
x_{TM} (km)	680	620 (640)	520	610 (660)	610 (660)
F_{MT} (erg/cm^2 s)	3.5 E6	7.3 E6 (5.7 E6)	1.5 E7	1.3 E7 (9.7 E6)	1.8 E7 (1.3 E7)
T_{TM} (K)	4540	4530 (4370)	4520	4450 (4300)	4230 (4250)
$d\bar{T}/dx$ (K/km)	4.1	3.4	2.1	2.5	1.8
x_{FD} (km)	740	680 (680)	590	670 (710)	680 (700)
M_S	1.44	1.46 (1.53)	1.48	1.77 (1.91)	2.10 (2.27)

As shown in Table 2 the mean intensity J oscillates around $\bar{J}$ with

$$\bar{J}=\frac{\sigma}{\pi}T_{RE}^4, \tag{13}$$

where T_{RE} is the radiative equilibrium temperature exhibited in Table 1. For the small amplitude waves at photospheric heights we have

$$\bar{B}=\frac{\sigma}{\pi}\bar{T}^4, \tag{14}$$

and thus $\bar{T}\simeq T_{RE}$. This shows that no physical temperature enhancement exists. The increased emission of the photosphere due to the radiative dissipation of the acoustic flux $\Delta F_M=F_{Mo}-F_{MT}=4.3$ E7 erg/cm^2 s for e.g. the wave with $P=30$ s and $F_{Mo}=5.0$ E7 erg/cm^2 s (c.f. Table 3) is produced by the waviness of the atmosphere. It is well known that a wavy atmosphere emits more energy than a smooth one. This is due to the fact that at large optical depth the emission is proportional to the curvature of the source function and at small optical depth to the optical distance between high and low temperature areas (Paper II). A striking example of the influence of waviness on the emission is the strong wavelength dependence of radiation damping (see Paper III) already found by Oster (1957) and Spiegel (1957). In empirical photospheric models which usually have a smooth dependence on height this waviness of the atmosphere and the resulting emission of the flux ΔF_M will however unavoidably be interpreted as due to a photospheric temperature enhancement. For estimates of this effect and a further discussion see Ulmschneider and Kalkofen (1973).

c) Temperature Depression Due to Nonlinearity

Near the temperature minimum as seen in Figs. 1, 2, 3, and 6 the time averaged temperature $\bar{T}$ is at first sight unexpectedly depressed below the radiative equilibrium temperature T_{RE} which at these heights [c.f. Eq. (1)] is equal to the boundary temperature $T_0=(\sqrt{3}/4)^{1/4}\,T_{eff}=4705$ K. The explanation of this effect which can also be seen in the entropy reduction rests again in the energy balance. At these heights where shocks have not yet formed there is mechanical heating due to radiation damping of the wave (Fig. 5). As seen in Table 2 the mean intensity J at these heights arising primarily from

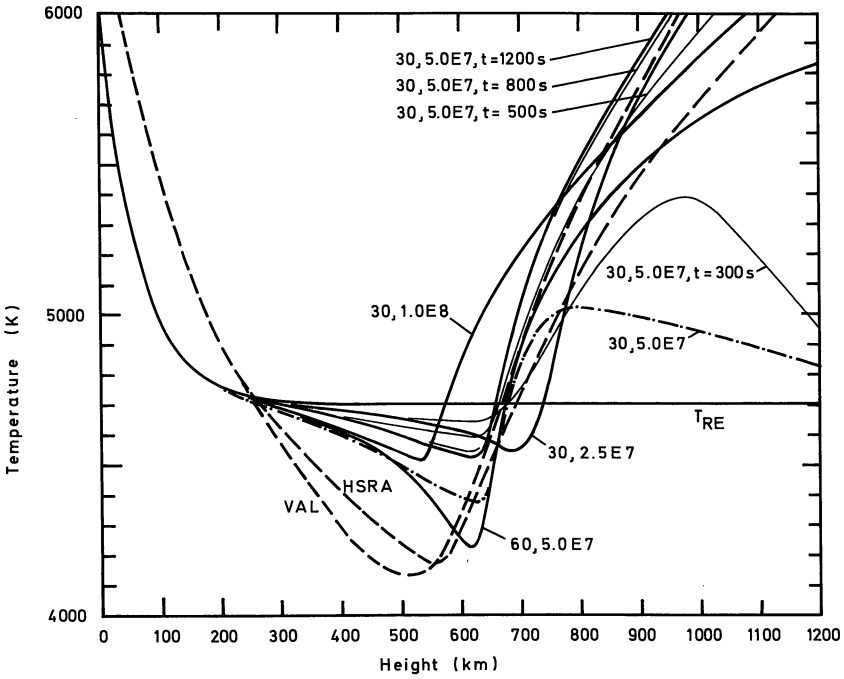

Fig. 6. Time averaged temperature $\bar{T}$ (drawn) as function of Euler height x for various acoustic waves of period P indicated in s and initial mechanical flux F_{Mo} indicated in erg/cm^{2}s. In one case the approach of the mean temperature (drawn thin) to steady state is shown for various times t. These calculations are for the opacity of Eq. (26). The influence of using Kurucz' (1978) opacities is shown (-.-.) for one case. The temperature distribution of the empirical HSRA (Gingerich et al., 1971) and VAL (Vernazza et al. 1976) models is shown dashed. T_{RE} is the initial radiative equilibrium temperature distribution

the region near $\tau=1$ is essentially constant. In the lower photosphere because of the small amplitude of the wave we have seen that T oscillates around T_{RE} which in the temperature minimum region is equal to the boundary temperature T_0. An important feature of our computation is however that the temperature oscillations at the temperature minimum region are *not* small ($\Delta T \simeq 500$ K see Fig. 2). Because of the strong temperature dependence of both the Planck function and the opacity we thus encounter effects due to the nonlinearity of these terms. In Eq. (11) in order to produce a specified radiative dissipation $\overline{dF_M/dx}$ of the mechanical flux (see Fig. 5) the right hand side must oscillate around a temperature $\bar{T}<T_0$ because the contribution to the r.h.s. for the temperature $\bar{T}+\Delta T$ is disproportionately larger than the contribution for $\bar{T}-\Delta T$. The exact amount of the temperature depression $\bar{T}-T_{RE}$ depends on the wave form, being smallest for saw tooth type and largest for sinusoidal type waves. Here the effect depends on the fraction of the wave period in which the wave stays in the high or low temperature state.

d) Limiting Shock Strength

Another interesting feature of Figs. 1 and 2 is that the temperature or velocity jump at the shock grows only very slowly after the shock is fully developed. The reason for this is that here shock dissipation counterbalances the steepening influence of the gravitational atmosphere. This property is well known from weak shock theory (see Ulmschneider, 1970) where shock waves in an isothermal gravitational atmosphere independent of their initial energy attain a limiting shock strength. Unfortunately weak shock theory is not applicable in our case because here the shock strengths are much too large. An attempt by Ulmschneider and Kalkofen (1978) who modify the weak shock theory to account for stronger shocks suffers from various stringent assumptions e.g. from the linear sawtooth approximation where the pressure and velocity profiles are both linear. However a number of interesting properties and similarities can be understood by comparison with these analytical approximations. The strength of the shock is usually described by the shock Mach number M_S which is defined (Landau Lifshitz, 1959, p. 331) by

$$M_S \equiv \frac{U-u_1}{c_1}, \tag{15}$$

where U is the shock velocity, u_1 is the gas velocity and c_1 the sound velocity both in front of the shock. These velocities are measured in the Euler frame. For the limiting shock strength the weak shock theory (Ulmschneider, 1970) predicts

$$M_S \equiv 1+\alpha = 1+\frac{\gamma g}{4 c_0} P. \tag{16}$$

Here γ is the ratio of specific heats and $c_0=(c_1+c_2)/2$ is the average sound velocity at the shock. For $P=30$, 45, 60 s and $T_0=5000$ K we find $M_S=1.51$, 1.75, 2.43 respectively. As seen in Figs. 1–3 and Table 3 this agrees quite well with the shock strengths found in our computations where with (Landau Lifshitz, 1959, p. 331)

$$\frac{p_2}{p_1} \equiv \phi = \frac{2\gamma M_S^2-\gamma+1}{\gamma+1}, \tag{17}$$

and

$$\frac{\rho_2}{\rho_1}\equiv\theta=\frac{(\gamma+1)M_S^2}{(\gamma-1)M_S^2+2}, \tag{18}$$

we have for the temperature, velocity and entropy jumps

$$\frac{T_2-T_1}{T_1}=\frac{\phi}{\theta}-1\simeq\alpha, \tag{19}$$

$$\frac{u_2-u_1}{c_1}=\frac{\theta-1}{\theta}M_S\simeq\frac{4\alpha}{\gamma+1}, \tag{20}$$

$$S_2-S_1=\frac{R}{\mu(\gamma-1)}\ln(\phi\theta^{-\gamma}). \tag{21}$$

Here subscripts 1 or 2 identify quantities in front of or behind the shock respectively.

e) Mass Loss and the Approach to a Steady State

The approach to steady state is shown in Fig. 4 by the height displacements of various fluid elements from their original Lagrange position. The times where shocks are transmitted at the upper boundary are also shown. It is seen that the first shock which travels into the undisturbed medium produces a large dissipation which causes the outer layers to expand rapidly overshooting the equilibrium positions. The atmosphere after the transmission of 12 shocks is already in steady state for heights less than 900 km. Greater heights reach steady state at progressively later times. This can be understood by considering the strong density decrease toward the outer layers. Small adjustments in lower denser layers will contribute considerably to the upper thinner layers. The upper boundary however does not seem to attain steady state. This is not expected as our shock waves have large amplitudes. Shock waves with large amplitudes are known to transport mass. The mass loss rate in our case can be computed from the drift of the upper boundary and the density at this point. We find from Fig. 4 $\overline{u_N}=3\ 10^7/9\ 10^2=3\ 10^4$ cm/s and with $\overline{\rho_N}=10^{-11}$ g/cm^3 a mass loss rate

$$\overline{\rho_N u_N}=3\text{ E-7 g/cm}^2\text{ s}. \tag{22}$$

In order not to deplete the slab of material taken for our computation this mass loss must be supplied at the piston in order to find a steady state. In our case with the lower boundary oscillating after Eq. (4) we do not allow any mass flow. The drift velocity $\overline{u_1}$ which must be added to the oscillating part of Eq. (4) is however only

$$\overline{u_1}=1\text{ cm/s}, \tag{23}$$

which is small compared with the errors made in our computation in view of the amplitude $u_0=1.8$ E4 cm/s. For the 60 s wave the mass loss rate is about a factor of 20 larger.

With the known Euler position of the lower boundary

$$x_1=a_1-\frac{u_0P}{2\pi}\left(1-\cos\frac{2\pi}{P}t\right), \tag{24}$$

a_1 being the Lagrange position of the lower boundary, and with the specific volume [Eq. (3) of Paper I] the Euler position of every Lagrange point can be computed. By interpolation to a given Euler grid an Euler frame calculation can be simulated. In the Euler frame the approach to steady state is more easily seen as this scheme does not concentrate on fluid particles which in the outer layers show perpetual motion towards regions of decreasing density. Fig. 6 shows the approach to steady state of the time averaged temperature $\bar{T}$ for various Euler positions. Once again, the progressively later approach to a steady state with increasing height is apparent.

f) Mechanical Flux and Dissipation, Amplification of the Acoustic Wave Due to the $\varkappa$-mechanism

Fig. 5 shows the time averaged acoustic flux as function of height for waves of different period P, initial flux F_{M_0} and opacity. There is a remarkable similarity to the results of Ulmschneider (1971b). After an initial decrease due to radiative damping the acoustic flux tends to become constant after the damping zone is passed. Approximate flux conservation leads to a rapid growth of the wave because of which, as indicated in Fig. 5, shocks form. Growth of the shock once more leads to a rapid decrease of the acoustic flux. The decrease of the acoustic flux due to radiative damping has been discussed in Sect. 3a and in Paper III. Short period waves suffer most severely from radiation damping. A striking feature of Fig. 5 is the constant logarithmic flux derivative of $(1/F_M)dF_M/dx=5.8$ E-8 cm^{-1} found for all waves. This behaviour starts roughly at the point x_{FD} where the shock is fully developed and the limiting shock strength is approximately reached. Fully developed here means that the shock connects the points of maximum and minimum wave amplitude. In Table 3 and Fig. 5 the heights x_{FD} are indicated together with the positions x_{SH} of shock formation. As already found by Ulmschneider (1971b) the difference between x_{SH} and x_{FD} is about 100–150 km. The constant logarithmic flux derivative for $x>x_{FD}$ is understood from the weak shock theory where at limiting shock strength (Ulmschneider, 1970, note printing error) one has

$$\frac{1}{F_M}\frac{dF_M}{dx}=\frac{\gamma g}{\gamma g/c_0^2}\simeq 8.6\text{ E-8 cm}^{-1}, \tag{25}$$

for $T=5000$ K. Ulmschneider (1971b) likewise finds a constant logarithmic flux derivative of $(1/F_M)dF_M/dx\simeq 6.5$ E-8 cm^{-1}. As opposed to the weak shock theory the acoustic flux for waves of limiting shock strength in our case is not $F_M\sim P^2$ but rather $\sim P$. This after

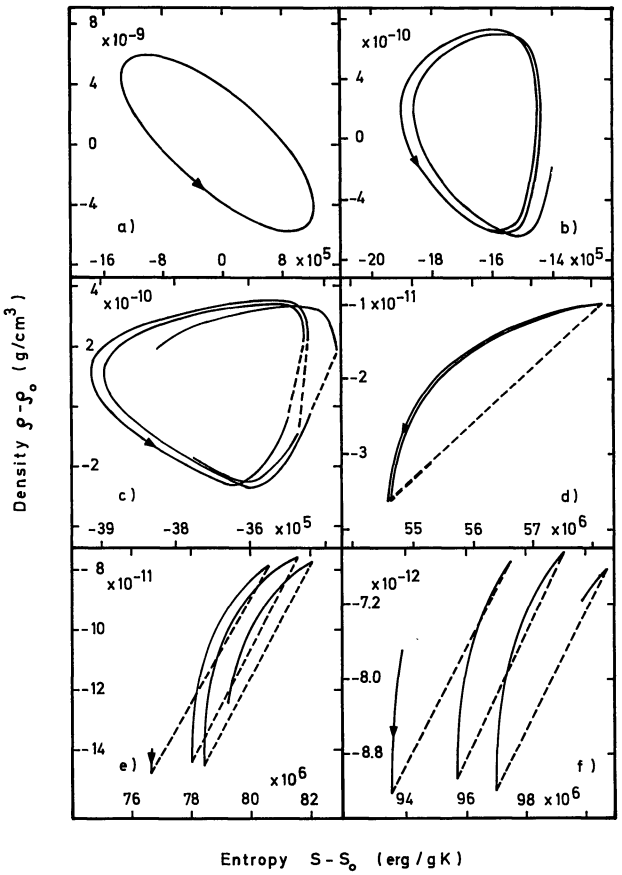

Fig. 7a—f. Thermodynamic cycles in the density entropy plane between times $t=1022$ and 1103 s of various gas particles, for the wave of $P=30$ s, $F_{Mo}=5.0$ E7 erg/cm^2 s and the opacity of Eq. (26). Values are shown relative to the initial state. The gas particles have the following Lagrange heights: **a** 94 km, **b** 468 km, **c** 624 km, **d** 966 km, **e** 1090 km, **f** 1150 km. The development of a Weyman path is demonstrated

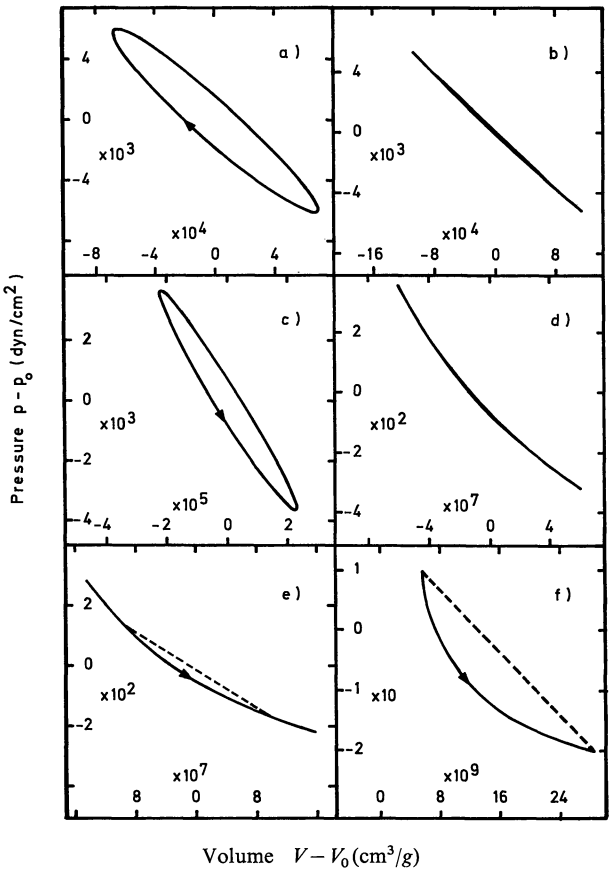

Fig. 8a—f. Thermodynamic cycles in the pressure volume plane between times $t=611$ and 829 s of various gas particles for the wave of $P=60$ s, $F_{Mo}=5.0$ E7 erg/cm^2 s and the opacity of Eq. (26). Values are shown relative to the initial state. The gas particles have the following Lagrange heights and optical depths: **a** −44 km; 3, **b** 11 km; 0.8, **c** 88 km; 0.2, **d** 550 km; 1E-4, **e** 616 km; 4E-5, **f** 946 km; 2E-7. For $\tau \geqq 1$ the cycles are in the positive work performing direction indicating amplification of the acoustic wave by the $\varkappa$-mechanism

Eq. (12) of Ulmschneider and Kalkofen (1978) is understood from the fact that $F_M \sim M_S - 1$ which after our present Eq. (12) is $\sim P$.

Another interesting property of the acoustic waves exhibited in Fig. 5 is the amplification of the acoustic flux at the region of optical depth $\tau \geqq 1$. As seen from Eq. (11) in order to have a positive flux derivative dF_M/dx, the number of photon absorptions J must be larger than the number of emissions B in the time mean. Near $\tau \geqq 1$ we find that for maximum temperature amplitude the emission is a maximum but the absorption, due to the large temperature dependence of the H^- opacity [c.f. Eq. (26)], is even greater. This effect is the well known $\varkappa$-mechanism (Baker and Kippenhahn, 1962; Baker, 1966 p. 338; Cox and Giuli, 1968 p. 1093). As discussed in Sect. 3h and shown in Fig. 8 we have confirmed this by plotting the thermodynamic cycle in the p-V plane.

g) Opacity and the Chromospheric Temperature Rise

Computations using the Kurucz (1978) opacity table but otherwise identical initial acoustic flux F_{Mo} and wave period P as seen in Figs. 1, 2, and 6 show considerable differences compared both to the computations using the approximate opacity of Eq. (26) and to empirical models like the HSRA (Gingerich et al., 1971) and the VAL (Vernazza et al., 1976) models. Undoubtedly some of this discrepancy is due to our grey radiation treatment. Another important cause for this discrepancy is the neglect of other, especially long period, components of the acoustic flux spectrum which preferentially heat the higher layers. A third significant reason is the assumption of LTE made both in our computation and in Kurucz's Table.

Undoubtedly there are important Non-LTE effects which reduce the source function and tend to decrease

Table 4. Grey absorption coefficient $\varkappa_A$ after Eq. (26) compared with the opacities $\varkappa_K$ of Kurucz (1978) and $\varkappa_G$ of Gingerich et al. (1971) as function of temperature T, pressure p and height h in the HSRA

h(km)	T(K)	p(dyn/cm^2)	$\varkappa_A$(g/cm^2)	$\varkappa_K$(g/cm^2)	$\varkappa_G$(g/cm^2)
1620	7360	3.763 E-1	1.44 E-4	3.24 E-1	8.63 E-2
1230	6180	3.793 E0	3.32 E-4	2.79 E-2	6.67 E-2
840	5300	6.750 E1	1.29 E-3	3.31 E-3	2.58 E-3
654	4660	3.375 E2	2.23 E-3	2.05 E-3	2.24 E-3
557	4170	8.682 E2	2.57 E-3	3.77 E-3	4.87 E-3
487	4250	1.768 E3	4.77 E-3	6.95 E-3	8.29 E-3
420	4380	3.457 E3	9.10 E-3	1.25 E-2	1.39 E-2
283	4660	1.269 E4	3.24 E-2	3.97 E-2	3.88 E-2
138	5160	4.562 E4	1.39 E-1	1.29 E-1	1.10 E-1
0	6390	1.310 E5	8.81 E-1	8.63 E-1	7.06 E-1

the local temperature sensitivity in favor of non local control by the entire atmospheric structure. This effect leads to a considerable decrease of the average emission which in our case as shown by the damping function D in Fig. 1 is concentrated primarily in high temperature areas immediately behind the shock. Moreover, non-LTE effects considerably change the relative importance of the principal chromospheric emitters (e.g. Cayrel effect). However a detailed time dependent non-LTE treatment of chromospheric emission as for example by Vernazza et al. (1976) is presently beyond the scope of this work.

To assess the effect of a different type of radiation loss on the chromospheric temperature rise we have made the simplifying assumption that chromospheric emission is due only to a few emitters among which H^- is the most important (see Athay, 1966; Ulmschneider, 1970, 1974; Ulmschneider and Kalkofen, 1978). This assumption is also suggested by the success in constructing chromosphere models with time independent means (Ulmschneider, 1971a; Kaplan et al., 1973). The H^- contribution was derived from Kurucz's (1978) opacity table by fitting a plane onto the H^- slope of the log $\varkappa$ versus log T, log p relation.

We find

$$\varkappa = 1.376\ \text{E-23}\ p^{0.738} T^5\ (\text{cm}^2/\text{g}). \tag{26}$$

This formula up to a constant factor of 20 closely resembles an expression for the grey surface absorption coefficient for Population I stars given by Stein (1966 p. 20). Table 4 gives a comparison of our approximate opacity values, $\varkappa_A$ of Eq. (26) with those of Kurucz (1978), $\varkappa_K$, and of Gingerich et al. (1971), $\varkappa_G$. It is seen that at high pressures a relatively good agreement between $\varkappa_A$ and $\varkappa_K$ or $\varkappa_G$ exists while at low pressures $\varkappa_A$ is smaller than $\varkappa_K$ especially for large temperatures.

Because $\varkappa_A$ and $\varkappa_G$ differ only at small pressures the initial radiative equilibrium atmosphere models as seen in Table 1 are almost identical except for the optical depth scale. Figs. 2 and 6 show a considerably increased chromospheric temperature rise if the opacity $\varkappa_A$ is used. The reason for this can be elucidated by considering the chromospheric energy balance. From Eq. (11) we find defining the mechanical source function

$$\bar{Q} \equiv -\frac{1}{4\pi\overline{\varkappa\rho}} \overline{\frac{dF_M}{dx}} = \bar{S} - \bar{J}, \tag{27}$$

where the time averaged radiative source function is given by

$$\bar{S} \equiv \frac{\sigma}{\pi} \bar{T}_c^4 \equiv \frac{\overline{\varkappa\rho B}}{\overline{\varkappa\rho}}, \tag{28}$$

and T_c is a chromospheric temperature.

Here because of the small optical depth after Table 2 we have

$$\bar{J} = \frac{\sigma}{\pi} T_0^4, \tag{29}$$

where $T_0 = 4705$ K as in Sect. 3c is the constant boundary temperature. Fig. 5 shows that independent of the opacity law, due to the limiting strength behaviour, a shock wave of given period at the same height approximately has the same dissipation rate. Thus Eqs. (27) to (29) show that the chromospheric temperature rise $\bar{T}_c - T_0$ depends primarily on the opacity $\overline{\varkappa\rho}$. For large $\overline{\varkappa\rho}$ as for the Kurucz opacity the mechanical source function at a given height is small and we must have $\bar{T}_c \simeq T_0$ as is shown in Figs. 1 and 6. In the case of Fig. 2 however where $\varkappa_A$ given by Eq. (26) is smaller than the Kurucz opacity $\varkappa_K$ we have a much larger mechanical source function and thus larger difference $\bar{T}_c - T_0$. It is interesting to note that in spite of the considerable difference in the chromospheric structure between Figs. 1 and 2 the shock strength and thus after Fig. 5 the mechanical dissipation is roughly the same at a given height or mean pressure. This indicates that the chromospheric temperature rise depends sensitively on the nature of the chromospheric emission which adjusts itself such that a given dissipated energy is emitted in the time mean. Fig. 6 shows the influence of both the initial acoustic

flux and the wave period on the chromospheric temperature rise.

The large discrepancy between our time averaged temperature $\bar{T}$ and the semi-empirical temperatures at heights $x<500$ km is due to our use of a grey opacity. Non grey treatment would considerably reduce this difference as seen in Fig. 20 of Vernazza et al. (1976). For a given period, as discussed in Paper III, the shock formation and consequently the temperature minimum occur at heights the lower the larger the initial acoustic flux. Here the temperature minimum unlike the results of our linearized work in Paper III, due to the temperature depression caused by the nonlinearity of the source function and opacity (c.f. Sect. 3*c*), is largely independent of the acoustic period and depends primarily on the initial acoustic flux. As shown in Table 3 and Fig. 6 the value of the minimum temperature however depends primarily on the wave period.

For waves of given period the chromospheric temperature gradient as seen in Table 3 and Fig. 6 is the steeper the smaller the initial acoustic flux. This is understood from Eqs. (27) to (29) by comparing the waves of $F_{\mathrm{Mo}}=1.0$ E8 and 2.5 E7 erg/cm^2 s where $P=30$ s. At the point of full shock development x_{FD} in Fig. 5 the acoustic dissipation $\overline{dF_M/dx}$ differs by about a factor of 5 while $\overline{\varkappa\rho}$ as seen from the optical depth scale by roughly a factor of 10.

h) Thermodynamic Cycle

Since a considerable span of years the thermodynamic cycle through which a gas particle moves in the presence of an acoustic shock wave is under discussion (see Bray and Loughhead, 1974). Schatzman (1949) assumes that after a gas particle is heated and compressed on crossing of the shock front it first expands adiabatically and then radiates back to its original condition. This cycle is known as Schatzman's path. Differently Weyman (1960) has postulated that after the compression by the shock the gas particle first radiates at constant density and then expands adiabatically back to the original state. This was henceforth called Weyman's path. Convenient plots of these cycles in the density, entropy plane are given by Bray and Loughhead (1974 p. 286, 289). It is interesting to see which one of these two cycles is realized for the short period waves of our work. Fig. 7 shows the thermodynamic cycle in the density ρ, entropy S plane for various mass particles of specified Lagrange height a for a wave with $P=30$ s and $F_{\mathrm{Mo}}=5$ E7 erg/cm^2 s. Either at small heights where the diffusion approximation is valid and where after Eq. (9) with Eq. (10) of Paper II, $D=dS/dt\sim d^2B/dt^2$, or in the photosphere where the optically thin approximation is valid and $D\sim -B$, we have a 180° phase shift between D and T and thus a 90° phase shift of T relative to S. With Eqs. (10) and (12) of Paper I, ρ depends on S and T such that, as exhibited by the inclined elliptical shape of the cycle in Fig. 7a, there is a phase shift of 135° of ρ relative to S. Near the temperature minimum the thermodynamic cycle is influenced by the strongly nonsinusoidal wave form. The compression region where the density rises quickly and almost adiabatically as seen in Figs. 7b, c gives the cycle a half circular shape. In this adiabatically rising part of the compression region the shocks develop. As weak shocks have a small entropy jump (Landau Lifshitz, 1959 p. 373) the discontinuity enters parallel to the ordinate (Fig. 7c). Increasing strength of the shock produces a larger entropy jump and the shock relative to the S axis becomes progressively less inclined. Fig. 7d exhibits a typical Weyman path. Figs. 7e, f show the effect of mass loss discussed in Sect. 3*e*. Here because the mass particle perpetually moves into areas of decreasing density the entropy increases secularly. Small changes in the entropy due to a not completely attained steady state are seen in Fig. 7c at the temperature minimum region where the point of shock formation as well as the adjacent rapid temperature rise reacts sensitively to small adjustments in the overall structure. The behaviour of a $P=60$ s wave is entirely similar to that of the $P=30$ s wave.

The thermodynamic cycle in the pressure P, volume V plane exhibited in Fig. 8 for the wave with $P=60$ s, $F_{\mathrm{Mo}}=5.0$ E7 erg/cm^2 s and the opacity of Eq. (26) illustrates the amplification and damping process. Fig. 8a at optical depth $\tau=3$ shows the cycle in a clockwise, positive work performing sequence similar to the cycles in the He convection zone of Christy (1966 p. 365, Fig. 7) which amplify the Cepheid pulsation with the γ-mechanism. In our case as also seen in Fig. 5 and discussed in Sect. 3*f*, positive work amplifies the acoustic wave with the $\varkappa$-mechanism (Baker and Kippenhahn, 1962; Baker, 1966 p. 338; Cox and Giuli, 1968 p. 1093) due to the large positive temperature dependence of the H^- opacity. Fig. 8b at $\tau\approx 1$ shows marginal work. Figs. 8c—f at $\tau<1$ exhibit counter-clockwise cycles with negative work performed by the gas particle signifying damping. Near the temperature minimum where radiative damping is smallest and shock dissipation is not yet important (see Fig. 5) the variation of p and V is roughly along an $S=$const adiabat (Fig. 8d). In this region the acoustic flux as a function of height is essentially conserved leading to a rapid growth of the wave amplitude and shock formation. Dissipation of a partially (Fig. 8e) and fully (Fig. 8f) developed shock wave again leads to considerable damping as also shown in Fig. 5.

i) Comparison with Time Independent Methods

The results of Jordan (1969), Ulmschneider (1971a), Kaplan et al. (1973), and Marik (1975) are based on the weak shock approximation which may be obtained from Eqs. (17) to (21) for $M_S=1+\alpha$ with small α. The validity

of this approximation can be tested e.g. in the expansion made for the shock dissipation in Eq. (21).

$$\ln(\phi\theta^{-\gamma}) \simeq \frac{16}{3}\frac{\gamma(\gamma-1)}{(\gamma+1)^2}\alpha^3, \tag{30}$$

which in our case with $\alpha \geqq 0.5$ is clearly not valid. The usage of the weak shock theory does however not invalidate the conclusions of Jordan (1969), Ulmschneider (1971), Kaplan et al. (1973) or of Marik (1975).

As shown by Ulmschneider and Kalkofen (1978) the energy balance between the H^- radiation loss and shock dissipation by short period waves is not much changed relative to the weak shock result if the shock treatment is improved. Thus a better treatment of shock propagation by Jordan (1969) or Ulmschneider (1971a) would very likely give similar agreement between theoretical and empirical chromospheres as is apparent in Fig. 6 of our present calculation. The same is valid for Kaplan et al. (1973) who in the chromosphere use the same formulae as Ulmschneider (1971). The unrealistically small height of the temperature minima of these authors is due to their large initial acoustic flux of between 3 E8 and 8 E9 erg/cm^2 s and their neglect of radiative damping. Thus their energy dissipated in the chromosphere is by about a factor of 50–1000 too large compared with the empirical value of about 6 E6 erg/cm^2 s. Using realistic acoustic fluxes and taking radiation damping into account, for instance after Paper III, Kaplan et al. (1973) would find agreement with the observed temperature minimum and could avoid to use their factor η. It is interesting to see that Kaplan et al. even with a very large overestimate of the acoustic flux find realistic chromospheric temperature rises.

4. Conclusions

Compared to the calculations discussed in Paper III the present work uses a grey radiative equilibrium model instead of semi-empirical models and the full radiation hydrodynamic method instead of the perturbation treatment. The main results of Paper III concerning the height of shock formation and the acoustic flux at this height have been confirmed in this work. It was found moreover that for the Sun the temperature minimum can roughly be identified with the shock formation point. The radiative dissipation of the acoustic flux up to the temperature minimum causes a photospheric temperature enhancement. It was found that this enhancement is produced by the waviness of the atmosphere and not by an actual temperature rise at the gas particles. In the low photosphere the time averaged temperature $\bar{T}$ is identical with the radiative equilibrium temperature T_{RE} of the initial atmosphere. At greater photospheric heights close to the temperature minimum a depression of $\bar{T}$ relative to T_{RE} becomes apparent which is due to the nonlinearity of the Planck function and the opacity produced by the large amplitude of the acoustic waves. This effect amounts to (c.f. Fig. 6) a depression of between $\Delta T = 200$ and 500 K and is the greater the larger the wave period. The shocks once formed grow rapidly and attain a limiting strength which increases with the period. The chromospheric shock strengths are rather large leading to temperature jumps of the order of 2000–5000 K. Independent of the initial flux, wave period or opacity law, the logarithmic derivative of the acoustic flux approaches a common limiting value while at a given height the acoustic flux of waves with identical initial flux is proportional to the period. As this flux is independent of the opacity law the chromospheric temperature is seen to adjust itself such that the emission balances the prescribed acoustic dissipation. The position of the chromospheric temperature rise depends on the point of shock formation which for a given period is determined by the initial acoustic flux F_{Mo} (see Paper III). Thus the larger the initial flux the lower the height of the chromospheric rise and the larger the gas pressure in the chromosphere. For similar acoustic periods, the chromospheric rise is found to be the steeper the smaller is the initial acoustic flux. A detailed comparison of chromospheric temperatures between empirical and theoretical models is however difficult and will not be attempted because of our restriction to grey radiation, to monochromatic acoustic waves and LTE. Nevertheless as Fig. 6 shows, empirical chromospheric temperature rises can easily be produced within a fairly large range of initial values of the acoustic flux and wave period. Amplification of the acoustic flux due to the $\varkappa$-mechanism is found but the effect is small because of the relatively small solar effective temperature. The large amplitudes of our waves produce mass loss from the upper layers. Here the mass loss rate was found to increase considerably with the period of the acoustic wave.

Appendix

A) Modifications in the Computation of Specific Intensities

As discussed in Paper II we usually interpolate the Planck function between grid or shock points by taking parabolas. Let us assume (c.f. Fig. 2 of Paper II) that we have a shock point (4, 5) very close to the grid point (3) and want to integrate the ingoing intensity I_4^- at shock point (4). Because of the closeness of points (3), (4) the source function would be poorly determined by a parabola through points (2), (3), and (4). Thus for the computation I_4^- we take a parabola through points (1), (2), and (4). For the outgoing intensity I^+ in the same case we use the parabola going through points (1), (2), and (4) to determine I_2^+. We then compute I_3^+ by taking a parabola through points (1), (2), and (3).

In cases where the shock is very close to the upper boundary or where a grid point has to be dropped because of closeness to the shock, less than three points remain between which the Planck function must be interpolated. In these cases we employ linear interpolation. Using the notation of Paper II we have

$$\delta_k^l \equiv \tau_l - \tau_k;\ \delta = \delta_i^{i+1};\ \delta_- = \delta_{i-1}^i. \tag{31}$$

We represent the source function S by linear segments

$$S(t) = S_i + (t-\tau_i)\frac{S_{i+1}-S_i}{\delta}. \tag{32}$$

Similar to Paper II we then find

$$I_i^+ - S_i^+ = (I_{i+1}^+ - S_{i+1}^+)e^{-\delta} + S_i^+ PO + S_{i+1}^+ PP, \tag{33}$$

with

$$PP = (1-e^{-\delta})/\delta;\ PO = -PP, \tag{34}$$

and

$$I_i^- - S_i^- = (I_{i-1}^- - S_{i-1}^-)e^{-\delta_-} + S_i^- QO + S_{i-1}^- QP, \tag{35}$$

with

$$QP = (1-e^{-\delta_-})/\delta_-;\ QO = -QP. \tag{36}$$

For cases where $\delta < 0.3$ or $\delta_- < 0.3$ we use expansions instead of Eqs. (34), (36).

B) Energy Balance in the Solar Atmosphere

Similar to Landau Lifshitz (1959, p. 11) we may derive an energy conservation equation in Lagrange form using Eqs. (2) to (7) of Paper I

$$\frac{\partial}{\partial t}\left(c_v T + \frac{1}{2}u^2 + g(x-a)\right) + \frac{\partial up}{\rho_0 \partial a} - T\left.\frac{dS}{dt}\right|_{\text{Rad}} = 0. \tag{37}$$

Here $c_v T$ is the internal energy, $\frac{1}{2}u^2$ the kinetic energy and $g(x-a)$ the gravitational energy per gram of a gas particle of mass $dm = \rho_0 da$ per square centimeter originally located at the height $x=a$. Here $x(a,t)$ is the Euler and "a" the Lagrange height. The acoustic flux F_M may be defined as

$$F_M \equiv up. \tag{38}$$

After Paper II we have for the derivative of the radiative flux

$$\frac{\partial F_R}{\partial a} = \frac{\rho_0}{\rho}\frac{\partial F_R}{\partial x} = -\rho_0 T\left.\frac{dS}{dt}\right|_{\text{Rad}}. \tag{39}$$

Thus Eq. (37) may be written

$$\frac{\partial}{\partial t}\left(c_v T + \frac{1}{2}u^2 + g(x-a)\right) + \frac{\partial}{\rho_0 \partial a}(F_M + F_R) = 0. \tag{40}$$

In steady state the pressure $p(a,t)$ and temperature $T(a,t)$ in the time mean approach limiting values $\bar{p}(a)$ and $\bar{T}(a)$. We thus have

$$p(a,t) = \bar{p}(a) + p'(a,t), \tag{41}$$

$$T(a,t) = \bar{T}(a) + T'(a,t). \tag{42}$$

The acoustic flux in steady state may be written as a sum of first and second order terms

$$F_M = F_M^{(1)} + F_M^{(2)}, \tag{43}$$

where

$$F_M^{(1)} \equiv u(a,t)\bar{p}(a) = \frac{\partial}{\partial t}x(a,t)\bar{p}(a), \tag{44}$$

represents work on the boundaries of the gas particle and where

$$F_M^{(2)} \equiv u(a,t)p'(a,t), \tag{45}$$

is the usually defined (Landau Lifshitz, 1959, p. 251) acoustic flux. Similarly in steady state the radiative flux may be written as a sum of first and second order terms

$$F_R = F_R^{(1)} + F_R^{(2)}, \tag{46}$$

where

$$F_R^{(1)} \equiv -\int \bar{T}(a)\left.\frac{dS}{dt}\right|_{\text{Rad}}(a,t)\rho_0(a)\,da, \tag{47}$$

describes the reversible exchange of photons between high and low temperature parts of the wave while

$$F_R^{(2)} \equiv -\int T'(a,t)\left.\frac{dS}{dt}\right|_{\text{Rad}}(a,t)\rho_0(a)\,da, \tag{48}$$

represents the radiative damping of the acoustic wave. The integrals in the last two equations have to be extended over $\Delta a = 1$ cm. Time averaging quantities in Eq. (40), we find that first order terms vanish together with the terms involving time derivatives (Landau Lifshitz, 1959, p. 252 footnote). We are thus left with the steady state energy conservation equation

$$\frac{\overline{dF_M}}{dx} + \frac{\overline{dF_R}}{dx} = \frac{\overline{dF_M^{(2)}}}{dx} + \frac{\overline{dF_R^{(2)}}}{dx} = 0. \tag{49}$$

References

Athay, R. G.: 1966, *Astrophys. J.* **146**, 223

Baker, N., Kippenhahn, R.: 1962, *Z. Astrophys.* **54**, 114

Baker, N.: 1966, Stellar Evolution, R. F. Stein, A. G. W Cameron Eds., Plenum Press, New York

Bray, R. J., Loughhead, R. E.: 1974, The Solar Chromosphere, Chapman and Hall, London

Christy, R. F.: 1966, Stellar Evolution, R. F. Stein, A. G. W. Cameron Eds., Plenum Press, New York

Cox, J. P., Giuli, R. T.: 1968, Stellar Structure, Gordon and Breach, London

Gingerich, O., Noyes, R. W., Kalkofen, W., Cuny, Y.: 1971, *Solar Phys.* **18**, 347

Hammer, R., Ulmschneider, P.: 1978, *Astron. Astrophys.* **69**, 273

Jordan, S.: 1969, NASA-Techn. Rept. TR R-291

Kalkofen, W., Ulmschneider, P.: 1977, *Astron. Astrophys.* **57**, 193

Kaplan, S. A., Ostrovskii, L. A., Petrukhin, N. S., Fridman, V. E.: 1973, *Soviet Astron.* **16**, 1013
Kurucz, R.: 1978, *Astrophys. J. Suppl.* (to be published)
Landau, L. D., Lifshitz, E. M.: 1959, Fluid Mechanics, Pergamon Press, London
Marik, M.: 1975, *Bull. Astron. Inst. Czech.* **26**, 317
Oster, L.: 1957, *Z. Astrophys.* **44**, 26
Schatzman, E.: 1949, *Ann. Astrophys.* **5**, 67
Spiegel, E. A.: 1957, *Astrophys. J.* **126**, 202
Stein, R. F.: 1966, Stellar Evolution, R. F. Stein, A. G. W. Cameron Eds., Plenum Press, New York
Ulmschneider, P.: 1970, *Solar Phys.* **12**, 403
Ulmschneider, P.: 1971a, *Astron. Astrophys.* **12**, 297
Ulmschneider, P.: 1971b, *Astron. Astrophys.* **14**, 275
Ulmschneider, P.: 1974, *Solar Phys.* **39**, 327
Ulmschneider, P., Kalkofen, W.: 1973, *Solar Phys.* **28**, 3
Ulmschneider, P., Kalkofen, W.: 1977, *Astron. Astrophys.* **57**, 199
Ulmschneider, P., Kalkofen, W.: 1978, *Astron. Astrophys.* (to be published)
Ulmschneider, P., Kalkofen, W., Nowak, T., Bohn, H. U.: 1977a, *Astron. Astrophys.* **54**, 61
Ulmschneider, P., Schmitz, F., Hammer, R.: 1978, *Astron. Astrophys.* (to be published)
Ulmschneider, P., Schmitz, F., Renzini, A., Cacciari, C., Kalkofen, W. and Kurucz, R.: 1977b, *Astron. Astrophys.* **61**, 515
Vernazza, J. E., Avrett, E. H., Loeser, R.: 1976, *Astrophys. J. Suppl.* **30**, 1
Weyman, R.: 1960, *Astrophys. J.* **132**, 452